



**HAL**  
open science

## Interface phenomena in ferromagnet/ $\text{TaO}_x$ -based systems: Damping, perpendicular magnetic anisotropy, and Dzyaloshinskii-Moriya interaction

I. Benguettat-El Mokhtari, Y. Roussigné, S. M. Chérif, A. Stashkevich, S. Auffret, C. Baraduc, M. Gabor, Hélène Béa, M. Belmeguenai

### ► To cite this version:

I. Benguettat-El Mokhtari, Y. Roussigné, S. M. Chérif, A. Stashkevich, S. Auffret, et al.. Interface phenomena in ferromagnet/ $\text{TaO}_x$ -based systems: Damping, perpendicular magnetic anisotropy, and Dzyaloshinskii-Moriya interaction. *Physical Review Materials*, 2020, 4 (12), pp.124408. 10.1103/PhysRevMaterials.4.124408 . hal-03094037

**HAL Id: hal-03094037**

**<https://hal.science/hal-03094037>**

Submitted on 27 Apr 2021

**HAL** is a multi-disciplinary open access archive for the deposit and dissemination of scientific research documents, whether they are published or not. The documents may come from teaching and research institutions in France or abroad, or from public or private research centers.

L'archive ouverte pluridisciplinaire **HAL**, est destinée au dépôt et à la diffusion de documents scientifiques de niveau recherche, publiés ou non, émanant des établissements d'enseignement et de recherche français ou étrangers, des laboratoires publics ou privés.

## Interface phenomena in ferromagnet/TaO<sub>x</sub>-based systems: Damping, perpendicular magnetic anisotropy, and Dzyaloshinskii-Moriya interaction

I. Benguettat-El Mokhtari,<sup>1,2</sup> Y. Roussigné<sup>1</sup>, S. M. Chérif<sup>1</sup>, A. Stashkevich,<sup>1</sup> S. Auffret,<sup>3</sup> C. Baraduc,<sup>3</sup> M. Gabor<sup>1,4</sup>, H. Béa<sup>3</sup>, and M. Belmeguenai<sup>1,\*</sup>

<sup>1</sup>Université Sorbonne Paris Nord, LSPM, CNRS, UPR 3407, F-93430 Villetaneuse, France

<sup>2</sup>Laboratoire de Physique des Couches Minces et Matériaux pour l'Electronique, Université Oran 1, BP1524, El M'naouar 31100 Oran, Algeria

<sup>3</sup>Université Grenoble Alpes, CEA, CNRS, Grenoble INP, IRIG, SPINTEC, F-38000 Grenoble, France

<sup>4</sup>Center for Superconductivity, Spintronics and Surface Science, Physics and Chemistry Department, Technical University of Cluj-Napoca, Memorandumului No. 28 RO-400114 Cluj-Napoca, Romania



(Received 3 September 2020; accepted 11 November 2020; published 21 December 2020)

Microstrip line ferromagnetic resonance (MS-FMR) and Brillouin light scattering (BLS) in the Damon-Eshbach geometry were used to investigate the perpendicular magnetic anisotropy (PMA), the damping and the interfacial Dzyaloshinskii-Moriya (iDMI) interaction in ferromagnetic (FM)/TaO<sub>x</sub>-based systems as a function of the ferromagnetic (FM = Co or Co<sub>8</sub>Fe<sub>72</sub>B<sub>20</sub>) and the TaO<sub>x</sub> thicknesses (oxidation level). The analysis of the experimental FMR and BLS data has shown that the effective magnetization, the Gilbert damping parameter  $\alpha$  and the iDMI are inversely proportional to the CoFeB and the Co films thickness. The BLS investigation of the iDMI variation versus the TaO<sub>x</sub> thickness and oxidation level reveals a contribution of FM/TaO<sub>x</sub> mediated by the presence of a Rashba field at this interface. Finally, we evidenced a correlation between iDMI and PMA by varying the Cu spacer thickness in the Pt/Cu/Co/TaO<sub>x</sub> system and we showed that both PMA and iDMI are localized at the first atomic monolayers of the Pt/Co interface. The observed non-linear dependence of PMA versus iDMI constant is attributed to similar interface orbital hybridizations involved in both quantities.

DOI: [10.1103/PhysRevMaterials.4.124408](https://doi.org/10.1103/PhysRevMaterials.4.124408)

### I. INTRODUCTION

The emergent interface induced phenomena yielding magnetic chiral structures [1–4] have broadened the interest of spintronics, especially for applications. This has triggered the potential development of new forms of spintronics chiral devices utilizing the reciprocal interactions of chiral structures with moving spin polarized electrons. A well-known example of such devices for ultradense, low-cost, and low-power storage technology is the racetrack memory, where skyrmions are manipulated through spin-orbit torque induced by the spin accumulation at the interface of ferromagnet and a heavy metal. Indeed, spin-orbit coupling (SOC) gives rise to a rapidly developing field of spinorbitronics and plays a crucial role in understanding the magnetization configuration [5]. Among interface SOC-related phenomena, a special attention to the interfacial Dzyaloshinskii-Moriya interaction (iDMI) is paid because of its asymmetrical character [6,7] yielding magnetic chiral configurations. The first prediction of iDMI for systems with broken inversion symmetry was purely based on a symmetry analysis, without referring to any specific physical effects [8]. In dielectrics lacking inversion symmetry, iDMI results from a combination of the SOC and the exchange interaction [9] while in metallic spin glasses containing nonmagnetic heavy metal (HM) im-

purities [10], the Ruderman-Kittel-Kasuya-Yosida (RKKY) interaction produces an indirect exchange interaction of the Dzyaloshinskii-Moriya type. This indirect exchange is due to the spin-orbit scattering of the conduction electrons by the nonmagnetic impurities.

The necessary symmetry reduction can be achieved at the interface in a bilayer made of ferromagnetic (FM) and heavy metal films. The iDMI mechanism is described by an elementary cell, referred to as Fert's triangle [11] involving two magnetic atoms and a SOC carrying atom on the heavy metal side. Thus the presence of SOC and a symmetry reduction, playing a determining role, are ensured [12]. The interfacial DMI can have another origin in relation with the Rashba interfacial coupling [13]. It was shown that the presence of a Rashba term in the Hamiltonian describing the interface between the ferromagnetic and the nonmagnetic layers is responsible for iDMI type interactions [14]. This term scales with the interface electric field, hence it will be more pronounced for combinations of materials of an entirely different physical nature, e.g., at the metal/insulator interface. This prediction has been verified experimentally by the observation of the generation of iDMI for interfaces including oxides, such as FeCoB/TaO<sub>x</sub> [15]. Despite recent theoretical efforts, both analytic and numerical, in an attempt to provide a reliable description of the microscopic origin of the iDMI [6,16,17], we are still far from a proper understanding. Further experimental investigation to perceive the underlying physics is thus still required. One of the effective ways to test the physical nature

\*belmeguenai.mohamed@univ-paris13.fr

of the interactions between the ferromagnetic and heavy metal atoms is by inserting a spacer between the FM and HM films thus isolating atoms in a Fert's triangle. The influence of a metallic spacer layer (Au and Ir) on iDMI and proximity induced magnetism has been recently investigated experimentally [18]. In particular, it was shown that an introduction of a Au or Ir monolayer (3–4 Å) leads to a characteristic threefold drop in iDMI strength, while a 12-Å one practically annihilates it. It has also been shown experimentally that even a slightly thinner Cu spacer (around 2 Å) brings about a similar threefold drop in DMI strength [19]. This cannot be easily reconciled with the concept of Fert *et al.*'s [11] triangle.

In this paper, we report the results of the experimental investigation of the influence of the ferromagnetic/oxide interface on different SOC-related parameters: perpendicular magnetic anisotropy, spin pumping-induced damping, and iDMI. We also investigate the nonmagnetic metallic spacer influence on these parameters. The studied structures are HM/FM/TaO<sub>x</sub>, where FM is a Co or CoFeB film with different thicknesses and HM = Pt or Ta, as well as Pt/SP/Co/TaO<sub>x</sub> where SP is a Cu film with various thicknesses. A series of Pt/Co/TaO<sub>x</sub> structures with different TaO<sub>x</sub> thicknesses have also been investigated.

## II. SAMPLES AND EXPERIMENTAL TECHNIQUES

In order to study the evolution of the magnetic properties in the HM/FM/TaO<sub>x</sub> system as a function of the different FM (FM = Co or Co<sub>8</sub>Fe<sub>72</sub>B<sub>20</sub>), HM (HM = Pt or Ta), TaO<sub>x</sub>, their thicknesses and their interface oxidation state, five sets of samples were grown at room temperature (RT) on thermally oxidized silicon (Si/SiO<sub>2</sub>) substrates by DC magnetron sputtering. In the first set, a Ta (3 nm) underlayer followed by Co<sub>8</sub>Fe<sub>72</sub>B<sub>20</sub> (CoFeB) of variable thickness ( $t_{\text{CFB}}$ ) ( $0.8 \text{ nm} \leq t_{\text{CFB}} \leq 10 \text{ nm}$ ) is deposited and then capped by Ta (0.8 nm). This latter is then oxidized in a treatment chamber (oxygen pressure of 150 mbar for 10 s). For surface protection of TaO<sub>x</sub>, a thin layer of Al (0.5 nm) is deposited after it. In the second set having the stack of Pt(3 nm)/Co( $t_{\text{Co}}$ )/TaO<sub>x</sub> (0.8 nm)/Al (0.5 nm), the Co thickness has been varied from 0.8 nm up to 10 nm. The CoFeB-based samples were annealed at 225 °C in vacuum for 30 min to improve the perpendicular magnetic anisotropy while the Co-based samples were not annealed in order to avoid the interdiffusion at the Pt/Co interface. For the two other systems having the structures of Pt(3 nm)/Co (1.2 nm)/TaO<sub>x</sub>( $t$ )/Al (0.5 nm) and Ta(3 nm)/CoFeB (1.15 nm)/TaO<sub>x</sub>( $t$ )/Al (0.5 nm), the thickness of TaO<sub>x</sub> was varied in the range of 0.6–1 nm. In the fifth set of samples, a Cu spacer layer of variable thickness in the range 0–2.4 nm has been inserted in the structure based on Co: Pt(3 nm)/Cu( $t_{\text{Cu}}$ )/Co (1.2 nm)/TaO<sub>x</sub> (0.8 nm)/Al (0.5 nm). For all the samples, the deposition is carried out in a chamber with a high base vacuum level in order to obtain a pure quality of the deposited materials (typically in the range of several 10<sup>-8</sup> mbar). The deposited thicknesses are determined by the opening time of the shutter that covers the target. The rates basically range between 0.03 and 0.1 nm/s, making it possible to deposit layers as thin as a few tenths of nanometers nominally. For the thinner cases, it may

correspond to a partial covering of the surface. The calibration of deposited thickness is made using films of thickness of typically 30 nm to have low error. The thickness of these thick films is measured using x-ray reflectivity. For film thickness in the nm range, deposition time is in the range of tens of seconds, which is still large with respect to the time for opening/closing the shutters for instance and we thus have enough accuracy in time of deposition. The typical error of thickness of one given sample is typically of 5–10%. The sputtering system is also equipped with a treatment chamber in which the natural oxidation takes place. Ta/FeCoB/TaO<sub>x</sub> is known to host skyrmions for applications in memory and logic devices [20] and Pt/Co-based samples are known to present a large iDMI, coming mainly from the Pt/Co interface.

The static magnetic properties of the samples were investigated using a vibrating sample magnetometer (VSM). Microstrip line ferromagnetic resonance (MS-FMR) [21] was used to determine the gyromagnetic ratio, the damping, and the perpendicular magnetic anisotropy (PMA) for the thicker films. Brillouin light scattering (BLS) [22], under in-plane applied magnetic field, was used in the Damon-Eshbach configuration to investigate the PMA (in samples where no significant or a weak MS-FMR signal is recorded) and iDMI in all the samples. The simultaneously detected Stokes (S) and anti-Stokes (aS) frequencies were determined from Lorentzian fit of BLS spectra. Two kinds of BLS experiments were performed: (i) measurements at fixed spin wave vector ( $4.1 \mu\text{m}^{-1}$ ) and variable in-plane applied magnetic fields to complete MS-FMR data for PMA investigation, and (ii) measurements at fixed in-plane saturating field and variable spin wave vector, needed to determine iDMI constant. For PMA investigation, the mean frequency  $[(F_S + F_{\text{aS}})/2]$  at fixed wave vector of  $4.1 \mu\text{m}^{-1}$  was studied as a function of the in-plane applied magnetic field. To characterize iDMI, the frequency mismatch ( $F_S - F_{\text{aS}}$ ), at fixed applied magnetic field, was investigated versus the spin wave (SW) vector.  $F_S$  and  $F_{\text{aS}}$  are taken in absolute values. All measurements to be presented below have been carried out at room temperature.

## III. RESULTS AND DISCUSSIONS

### A. Effect of the ferromagnetic thickness

#### 1. VSM measurements

For interface phenomena, the estimation of the magnetic dead layer thickness ( $t_d$ ) is essential, since the effective thickness of the ferromagnetic layer can be reduced due to the diffusion of atoms at interface. Besides  $t_d$ , magnetization at saturation  $M_s$  is also needed for the characterization of these interface effects. For this, the vibrating sample magnetometer (VSM) technique was exploited to measure the saturation magnetic moment per unit area ( $M_s \times t_{\text{FM}}$ ), versus the ferromagnetic thicknesses ( $t_{\text{FM}}$ ) for Ta/CoFeB/TaO<sub>x</sub> and Pt/Co/TaO<sub>x</sub> stacks as shown in Fig. 1. The linear fit of these data gives straightforwardly  $M_s$  and  $t_d$  from the slope and the horizontal axis intercept, respectively. The lower magnetization at saturation ( $M_s = 1230 \pm 50 \text{ emu/cm}^3$ ) for Pt/Co/TaO<sub>x</sub> with respect to that of bulk Co is most likely attributed to a partial oxidation of the Co at the Co/TaO<sub>x</sub> interface and to oxygen contamination of the Co layer volume. As

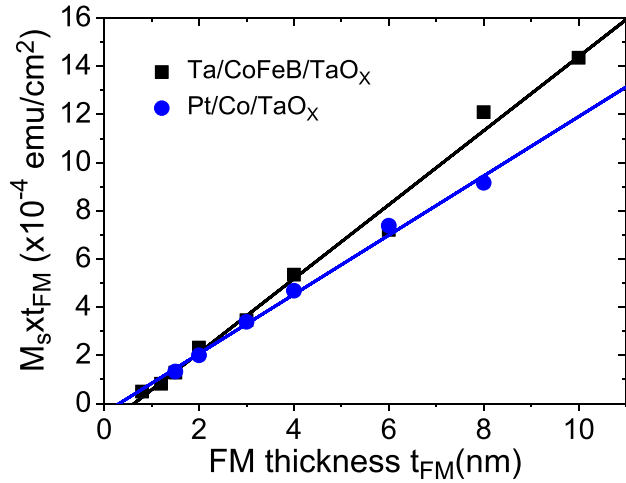


FIG. 1. Saturation magnetic moment per unit area vs FM thickness (where FM = Co<sub>8</sub>Fe<sub>72</sub>B<sub>20</sub> or Co) of FM-based systems with Pt or Ta buffer and TaO<sub>x</sub> capping layers. Symbols refer to the VSM measurements and solid lines are the linear fits.

it was previously shown for Pt/Co/MgO [23], oxygen atoms can migrate through the interface into the volume and contaminate the Co layer, resulting in a decrease of the  $M_s$  which is correlated with the degree of the oxygen contamination [24]. For the Ta/CoFeB/TaO<sub>x</sub> system, the obtained high value of  $M_s$  ( $M_s = 1536 \pm 60$  emu/cm<sup>3</sup>) is most probably due the CoFeB composition which is rich in Fe, known to have high  $M_s$ . This  $M_s$  value is higher than those of Co<sub>20</sub>Fe<sub>60</sub>B<sub>20</sub> ( $M_s = 1380$  emu/cm<sup>3</sup> [25]) and Co<sub>40</sub>Fe<sub>40</sub>B<sub>20</sub> ( $M_s = 1350$  emu/cm<sup>3</sup> [26]). However, the Fe composition dependence of  $M_s$  in (Co<sub>1-x</sub>Fe<sub>x</sub>)<sub>80</sub>B<sub>20</sub>, with the Fe composition in the range  $x = 0.3-1.0$ , investigated by Ogasawara *et al.* [27], revealed that  $M_s$  is higher than 1500 emu/cm<sup>3</sup> for all the investigated  $x$  values.

The magnetic dead layer thickness is estimated to be  $0.7 \pm 0.1$  nm and  $0.3 \pm 0.1$  nm, respectively for Ta/CoFeB/TaO<sub>x</sub> and Pt/Co/TaO<sub>x</sub>. This magnetic dead layer could originate from the intermixing of the heavy metal (Pt or Ta) and FM layer at the bottom interface, oxidation of the FM layer when the top HM layer is too thin, and intermixing of the top metal and the FM layer (top interface) when the top metal is not adequately oxidized. It is worth mentioning that Fe is more sensitive to O than Co. Therefore, the higher magnetic dead layer for Ta/CoFeB/TaO<sub>x</sub> is more probably due to higher oxidation at the top interface of CoFeB and probably to an additional intermixing at the Ta/CoFeB bottom interface, since no magnetic dead layer was observed for Pt/Co/Pt systems [24]. Indeed, Ta at the interface with FeCoB is known to result in a dead layer (of the order of 0.3 nm [15]), which is supported by *ab initio* calculations [28], showing a decrease of Fe magnetization. Following the determination of  $t_d$ , we then consider the effective thickness of the CoFeB and the Co ( $t_{\text{eff}}$ ) as the nominal FM thickness reduced by the thickness of the magnetic dead layer:  $t_{\text{eff}} = t_{FM} - t_d$ . In the following, all parameters will be discussed as a function of this effective thickness unless explicitly mentioned.

## 2. BLS and MS-FMR measurements

In this section, the focus is made on the investigation of PMA constants, the iDMI strength, and the spin pumping-induced damping as a function of the FM thickness in Co- and CoFeB-based systems. For this purpose the measurement of the  $g$  factor and therefore, the gyromagnetic ratio  $\gamma$  determination is essential. This  $g$  factor is precisely determined via the MS-FMR technique through the study of the uniform precession mode frequency ( $F_{\perp}$ ) versus the perpendicular to the film plane applied magnetic field ( $H_{\perp}$ ). Thus,  $(\gamma/2\pi)$  is directly deduced after fitting the experimental data as shown in Fig. 2(a) for 2-nm-thick CoFeB and 3-nm-thick Co films using Eq. (1) [29],

$$F_{\perp} = \frac{\gamma}{2\pi} (H_{\perp} - 4\pi M_{\text{eff}}), \quad (1)$$

where  $4\pi M_{\text{eff}} = 4\pi M_s - \frac{2K_{\perp}}{M_s}$  is the effective magnetization,  $K_{\perp}$  is the perpendicular uniaxial magnetic anisotropy constant, and  $\gamma$  is the gyromagnetic ratio [ $\gamma/(2\pi) = g \times 13.97$  GHz/T].

Note that in the above equation, since the resonance fields under perpendicular applied magnetic fields overpass 5 kOe, the magnetic in-plane anisotropy fields, which are expected to be much smaller, as shown in the next paragraph, are then neglected. The  $g$ -factor value is found to be  $2.07 \pm 0.01$  ( $\gamma/2\pi = 2.886 \pm 0.014$  MHz/Oe) and  $2.22 \pm 0.21$  ( $\gamma/2\pi = 3.10 \pm 0.03$  MHz/Oe), respectively for the Ta/CoFeB/TaO<sub>x</sub> and the Pt/Co/TaO<sub>x</sub> systems. Note that for the very thin Co and CoFeB films (below 2 nm) the MS-FMR signal amplitude decreases, the signal becomes undetectable, and the  $g$  factor cannot be determined. Moreover, for the thickest Co and CoFeB films, high magnetic resonance fields beyond 15 kOe (the maximal applied magnetic field available in our MS-FMR setup) are needed to have experimental data over a large enough frequency range to precisely determine the  $g$ -factor. Therefore, the measurements of the  $g$  factor were restricted to a limited range of the FM thickness and the above mentioned values of  $g$  factor were used for all the FM thicknesses of the corresponding systems used here.

For an accurate determination of the effective magnetization, the in-plane magnetic anisotropy was studied by measuring the variation of the resonance field for the direction of the applied magnetic field ( $H_{//}$ ) with the substrate edges ( $\varphi_H$ ) at a fixed driving frequency. Figure 2(b) shows the typical angular dependences at 8 GHz driving frequency for both Ta/CoFeB/TaO<sub>x</sub> and Pt/Co/TaO<sub>x</sub> at various FM thicknesses, revealing a small uniaxial anisotropy with the magnetization easy axis direction depending on the sample. To quantify the uniaxial magnetic anisotropy field ( $H_u$ ), the angular dependence, shown in Fig. 2(b), was fitted with Eq. (2) [29],

$$f_{//}^2 = (\gamma/2\pi)^2 [H_{//} \cos(\varphi_M - \varphi_H) + H_u \cos 2(\varphi_M - \varphi_u)] \times \left( H_{//} \cos(\varphi_M - \varphi_H) + 4\pi M_{\text{eff}} + \frac{H_u}{2} [1 + \cos 2(\varphi_M - \varphi_u)] \right), \quad (2)$$

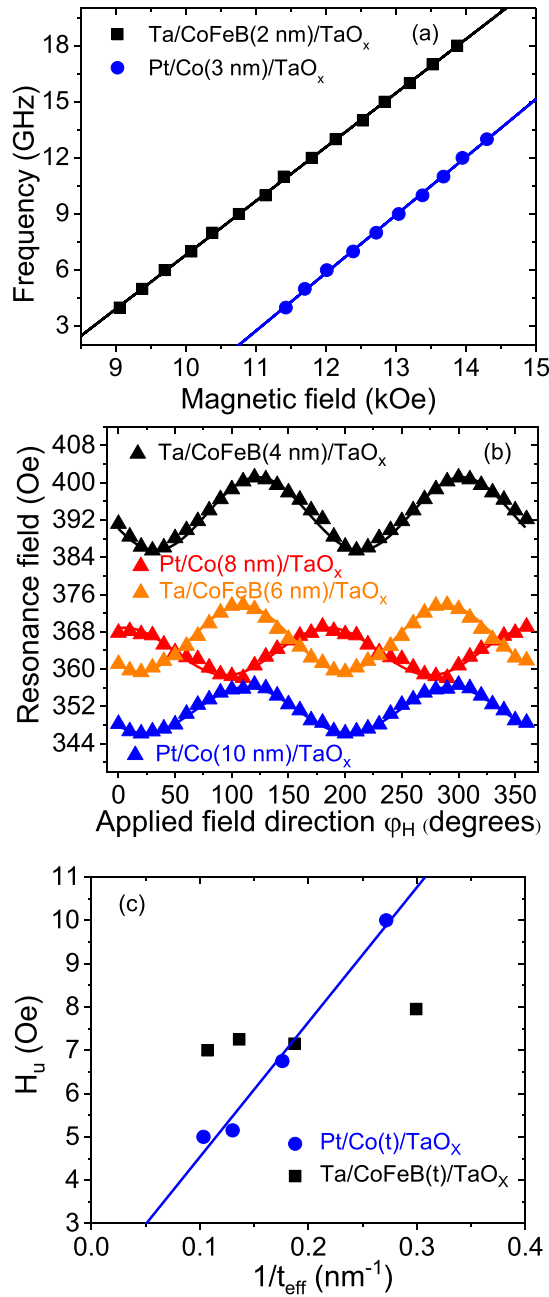


FIG. 2. (a) Variations of the uniform precession mode frequency vs the perpendicular to the film plane applied magnetic field for  $\text{CoFeB}(t_{\text{CFB}})/\text{Pt}$ . Symbols refer to experimental data and solid lines are fits using Eq. (1). (b) FMR resonance field vs the direction of the in-plane applied magnetic field with respect to the substrate edge ( $\varphi_H$ ) measured at 8 GHz driving frequency for FM-based systems (where FM =  $\text{Co}_8\text{Fe}_{72}\text{B}_{20}$  or Co) with Pt or Ta buffer and  $\text{TaO}_x$  capping layers. Symbols refer to experimental data and solid lines are fits using Eq. (2). (c) Variations of the uniaxial anisotropy field as a function of reciprocal effective thicknesses ( $1/t_{\text{eff}}$ ) of CoFeB or Co in  $\text{Ta}/\text{CoFeB}/\text{TaO}_x$  and  $\text{Pt}/\text{Co}/\text{TaO}_x$  systems. Symbols are experimental data and the solid line refers to the linear fit.

where  $\varphi_M$  is the in-plane direction of the magnetization and  $\varphi_u$  is the angle of the easy axis direction of the uniaxial anisotropy with the substrate edges.

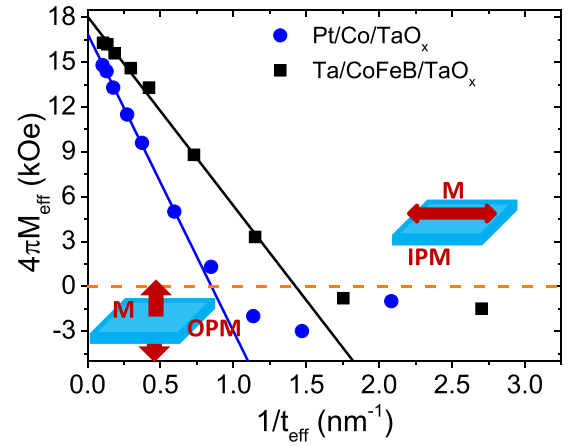


FIG. 3. Effective magnetization ( $4\pi M_{\text{eff}}$ ) vs the reciprocal effective thickness of Co or CoFeB ( $1/t_{\text{eff}}$ ) in  $\text{Pt}/\text{Co}/\text{TaO}_x$  and  $\text{Ta}/\text{CoFeB}/\text{TaO}_x$  systems.  $4\pi M_{\text{eff}}$  values have been extracted from the fit of MS-FMR or BLS measurements under in-plane applied magnetic fields. Symbols refer to experimental data while solid lines are the linear fits.

The variations of  $H_u$  versus the reciprocal effective thickness of the FM layers ( $1/t_{\text{eff}}$ ), shown in Fig. 2(c), reveal that while  $H_u$  of the  $\text{Ta}/\text{CoFeB}/\text{TaO}_x$  system remains mostly constant, a clear linear behavior can be observed for the  $\text{Pt}/\text{Co}/\text{TaO}_x$ , suggesting an interfacial contribution to this uniaxial anisotropy. The derived uniaxial in-plane surface anisotropy constant ( $1.9 \times 10^{-3}$  erg/cm<sup>2</sup>) is in good agreement with that of the annealed  $\text{Co}_{20}\text{Fe}_{60}\text{B}_{20}/\text{Pt}$  [29]. The precise origin of this interface uniaxial anisotropy is not clear, however since it is observed only for  $\text{Pt}/\text{Co}/\text{TaO}_x$  and previously for  $\text{Co}_{20}\text{Fe}_{60}\text{B}_{20}/\text{Pt}$  it is most probably induced by Pt.

Once the direction of the uniaxial in-plane magnetic anisotropy easy axis is identified, the resonance field dependence of the microwave driving frequency was measured for each sample and then fitted with Eq. (2) to deduce  $M_{\text{eff}}$  as shown in Fig. 3. For samples where the MS-FMR signal is not enough to be detected, BLS measurements were used to determine  $M_{\text{eff}}$  as described in [30]. Positive values of  $M_{\text{eff}}$  correspond to in-plane spontaneously magnetized films (IPM) while negative values refer to out-of-plane spontaneously magnetized samples (OPM). Figure 3 shows that the perpendicular to the film plane magnetization easy axis (spontaneous perpendicular magnetized) is obtained for  $t_{\text{Co}} \leq 1.4$  nm and for  $t_{\text{CFB}} \leq 1.3$  nm. The 0.8-nm-thick CoFeB layer did not show any BLS signal suggesting that it is paramagnetic, in good agreement with the thicker magnetic dead layer for the  $\text{Ta}/\text{CoFeB}/\text{TaO}_x$  system. Figure 3 also reveals that  $M_{\text{eff}}$  varies linearly with the reciprocal effective thickness of the FM layer for both systems. Note the deviation of the  $M_{\text{eff}}$  from the linear dependence for FM nominal thicknesses below 1.5 nm for both systems, most probably due to the degradation of interfaces of thinner FM layers. Therefore, the linear fits of data in Fig. 3 (for nominal FM thicknesses above 1.5 nm) were used to determine the perpendicular uniaxial surface  $K_s$  and volume  $K_v$  anisotropy constants from the slope and the intercept with the vertical axis, since  $K_{\perp}$  obeys the relation  $K_{\perp} = K_v + \frac{K_s}{t_{\text{eff}}}$ . As summarized in Table I,  $K_s$  of

TABLE I. Parameters obtained from the best fits of the thickness dependencies of the magnetic moment per area unit, the effective magnetization, and damping of the CoFeB- and Co-based systems grown on Si substrates using Ta or Pt buffer layers and TaO<sub>x</sub> capping layer.

System	$M_s$ (emu/cm <sup>3</sup> )	$t_d$ (nm)	$K_s$ (erg/cm <sup>2</sup> )	$K_v$ ( $\times 10^6$ erg/cm <sup>3</sup> )	$g_{\text{eff}}^{\uparrow\downarrow}$ (nm <sup>-2</sup> )	$D_s$ ( $\times 10^{-7}$ erg/cm)	$\alpha_{\text{FM}}$ ( $\times 10^{-3}$ )
Pt/Co/TaO <sub>x</sub>	1230 $\pm$ 50	0.3 $\pm$ 0.1	1.22 $\pm$ 0.06	-0.89 $\pm$ 0.04	30.05 $\pm$ 2.3	-1.25 $\pm$ 0.05	8.40 $\pm$ 0.34
Ta/CoFeB/TaO <sub>x</sub>	1536 $\pm$ 60	0.7 $\pm$ 0.1	0.97 $\pm$ 0.09	0.95 $\pm$ 0.05	14.5 $\pm$ 1.2		3.1 $\pm$ 0.2

Pt/Co/TaO<sub>x</sub> ( $K_s = 1.22 \pm 0.06$  erg/cm<sup>2</sup>) is higher than that of Ta/CoFeB/TaO<sub>x</sub> ( $K_s = 0.97 \pm 0.09$  erg/cm<sup>2</sup>) most probably due to the better interface quality of the Pt/Co interface presenting a thinner magnetic dead layer than Ta/CoFeB. We should mention that measurements (not shown here) on CoFeB/TaO<sub>x</sub> systems (systems without a Ta buffer layer) revealed a higher  $K_s$ , confirming the degradation of the interface anisotropy by the Ta buffer layer. This interface PMA is most likely due to the interfacial hybridization resulting in strong spin-orbit interaction between the magnetic and nonmagnetic metals:  $3d$  orbitals of Fe and Co and  $2p$  of O (for the top interface) and  $5d - 3d$  hybridization for bottom interfaces [31]. The volume contribution ( $K_v$ ) is found to be small compared to the overall magnetic anisotropy. It is negative for Pt/Co/TaO<sub>x</sub> [ $K_v = -(0.89 \pm 0.04) \times 10^6$  erg/cm<sup>3</sup>], reinforcing the in-plane magnetic easy plane. The weaker  $K_v$  (in absolute value) than the magnetocrystalline anisotropy of hexagonal Co ( $K_v = 5.3 \times 10^6$  erg/cm<sup>3</sup>) [32] and its negative sign could be attributed to defects in the film, like strains, and disorder, due to the interdiffusion in the Co volume. It is worth mentioning the positive and the higher  $K_v$  value [ $K_v = (0.95 \pm 0.05) \times 10^6$  erg/cm<sup>3</sup>] obtained for Ta/CoFeB/TaO<sub>x</sub>, which is comparable to that of the bulk bcc-Fe ( $0.45 \times 10^6$  erg/cm<sup>3</sup>) [33].

We also investigated the magnetic damping control via the FMR-induced spin pumping, where the precession of the magnetization around the effective field generates a spin current which diffuses into the adjacent nonmagnetic layer and is accompanied by an increase in the damping coefficient of the FM layer. For this, MS-FMR was used to measure the half width at half maximum linewidth ( $\Delta H$ ), deduced from the Lorentzian derivative fit of MS-FMR spectra, versus the microwave driving frequency and as a function of  $\phi_H$ . Since  $\Delta H$  results from extrinsic and intrinsic contributions to damping, the angular dependence of  $\Delta H$  [Fig. 4(a)] is used to determine the direction of the applied magnetic field giving the minimal  $\Delta H$  value, where the extrinsic contributions to the linewidth are minimal. The frequency dependence of  $\Delta H$  along this direction is then measured and fitted by Eq. (3) leading to the determination of the Gilbert damping parameter  $\alpha$ , as shown in Fig. 4(b) for both Pt/Co/TaO<sub>x</sub> and Ta/CoFeB/TaO<sub>x</sub> systems,

$$\Delta H = \Delta H_0 + \frac{\alpha}{\gamma} 2\pi f, \quad (3)$$

where  $f$  is the driving frequency and  $\Delta H_0$  is the inhomogeneous residual linewidth, which is frequency independent.

Figure 4(c) reveals that the obtained damping constant increases linearly with  $1/t_{\text{eff}}$  due to the spin pumping-induced current in Pt and Ta by the FMR precession of the magnetization. Therefore, the total damping results from a bulk

contribution, intrinsic to the FM material ( $\alpha_{\text{FM}}$ ), and additional damping ( $\Delta\alpha$ ) caused by the spin pumping, which varies linearly versus  $1/t_{\text{eff}}$  as given by Eq. (4) [34],

$$\alpha = \alpha_{\text{FM}} + \Delta\alpha = \alpha_{\text{FM}} + \frac{g\mu_B}{4\pi M_s} g_{\text{eff}}^{\uparrow\downarrow} \frac{1}{t_{\text{eff}}}, \quad (4)$$

where  $\mu_B$  is the Bohr magneton and  $g_{\text{eff}}^{\uparrow\downarrow}$  is the effective spin mixing conductance.

The linear fit of the experimental data of Fig. 4(b) gives  $\alpha_{\text{CoFeB}} = (3.1 \pm 0.2) \times 10^{-3}$  for Ta/CoFeB/TaO<sub>x</sub> and  $\alpha_{\text{Co}} = 8.40 \times 10^{-3}$  for the Pt/Co/TaO<sub>x</sub> (see Table I) and allows us to determine  $g_{\text{eff}}^{\uparrow\downarrow}$ . The obtained value of  $\alpha_{\text{CoFeB}}$  is slightly higher than that of the bulk Fe ( $1.9 \times 10^{-3}$ ) [35] and is comparable to the reported one for Co<sub>20</sub>Fe<sub>60</sub>B<sub>20</sub> ( $3.4 \times 10^{-3}$ ) [29]. Moreover, the obtained value of  $\alpha_{\text{Co}}$  [ $(8.40 \pm 0.34) \times 10^{-3}$ ], which is in good agreement with that of Co hcp ( $8 \times 10^{-3}$ ) reported by Devolder *et al.* [36], suggests that Co films are hcp. Note again the lower  $g_{\text{eff}}^{\uparrow\downarrow}$  value ( $14.5 \pm 1.2$  nm<sup>-2</sup>) of Ta/CoFeB/TaO<sub>x</sub> system, suggesting lower spin pumping efficiency. The obtained value of the  $g_{\text{eff}}^{\uparrow\downarrow}$  of Pt/Co/TaO<sub>x</sub> system ( $30 \pm 2.3$  nm<sup>-2</sup>) is lower than the ones reported by Zhang *et al.* ( $39.6$  nm<sup>-2</sup>) [37] and by Pai *et al.* ( $53$  nm<sup>-2</sup>) [38]. For this latter, authors explained the large value of  $g_{\text{eff}}^{\uparrow\downarrow}$  as a result of some mechanism other than spin pumping into Pt through an abrupt, reasonably well ordered Pt/FM interface. The lower  $g_{\text{eff}}^{\uparrow\downarrow}$  of Ta/CoFeB/TaO<sub>x</sub> compared to Pt/Co/TaO<sub>x</sub> could be attributed to the stronger intermixing at the CoFeB interfaces resulting in a relatively wide interface region which may kill the abrupt potential change at interfaces. Therefore, conduction electrons across the interface are less scattered, resulting in small interface spin losses [39] leading to a higher spin back flow and thus lower  $g_{\text{eff}}^{\uparrow\downarrow}$ .

BLS spectra were also measured as a function of the SW vector ( $k_{\text{SW}}$ ) and under in-plane applied magnetic field, high enough to saturate the magnetization in the film plane, as shown in Fig. 5(a) for some Co thicknesses of the Pt/Co/TaO<sub>x</sub> system and for  $k_{\text{SW}} = 20.45 \mu\text{m}^{-1}$ . Besides lines position and linewidth variations with  $t_{\text{Co}}$ , due to PMA and spin pumping, spectra reveal also a frequency difference between S and aS lines. This frequency mismatch, defined as  $\Delta F = F_S - F_{aS}$ , varies linearly with  $k_{\text{SW}}$  as shown in Fig. 5(b) and is field independent, for saturating fields [see inset of Fig. 5(b)]. This frequency difference, traducing the SW propagation non-reciprocity, is induced by iDMI at interfaces with Co. To characterize the iDMI strength, the effective constant ( $D_{\text{eff}}$ ) was calculated from the fit of the experimental dependence of  $\Delta F$  versus  $k_{\text{SW}}$  using Eq. (5),

$$\Delta F = F_S - F_{aS} = D_{\text{eff}} \frac{2\gamma}{\pi M_s} k_{\text{SW}} = \frac{D_s}{t_{\text{eff}}} \frac{2\gamma}{\pi M_s} k_{\text{SW}}. \quad (5)$$

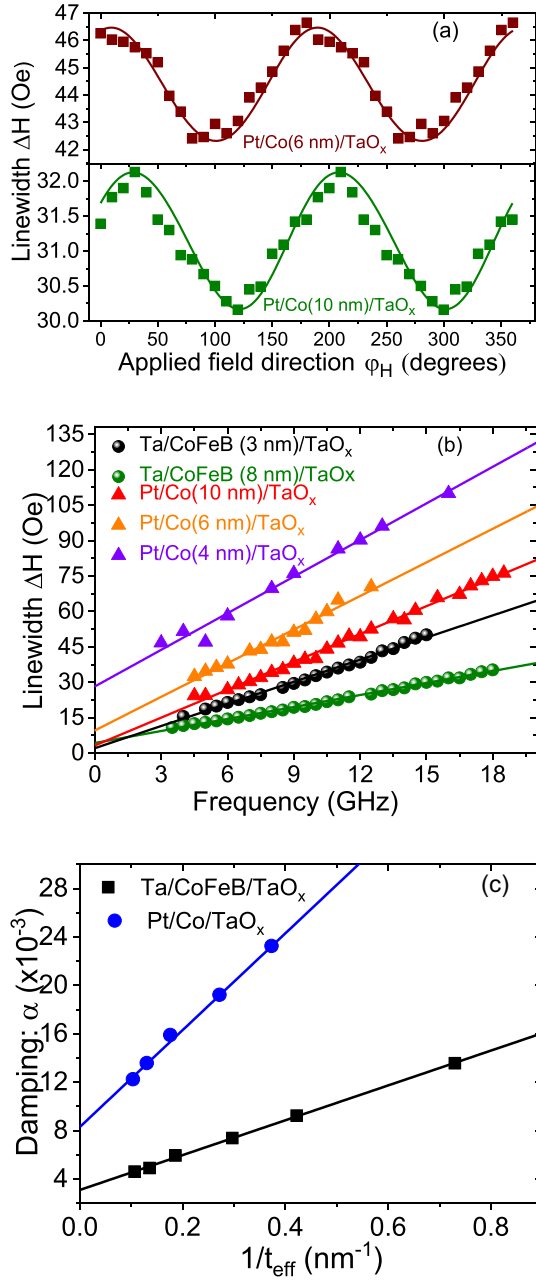


FIG. 4. (a) Dependence of the FMR half width at half maximum linewidth ( $\Delta H$ ) vs the direction of the in-plane applied magnetic field with respect to the sample edge ( $\phi_H$ ) measured at 8 GHz driving frequency for Pt/Co(10 and 6 nm)/TaO<sub>x</sub> systems. Symbols refer to experimental data and solid lines are fits using model in [21]. (b) Frequency dependence of  $\Delta H$  for Ta/CoFeB/TaO<sub>x</sub> and Pt/Co/TaO<sub>x</sub> systems with various CoFeB and Co thicknesses. Symbols refer to experimental data and solid lines are fits using Eq. (3). (c) Gilbert damping constant as a function of the reciprocal CoFeB and Co effective thickness for Ta/CoFeB/TaO<sub>x</sub> and Pt/Co/TaO<sub>x</sub> systems. Symbols refer to experimental data and solid lines are fits using Eq. (4).

The thickness dependence of  $D_{\text{eff}}$  is shown in Fig. 5(c) for Pt/Co/TaO<sub>x</sub>, where a linear dependence versus  $1/t_{\text{eff}}$  is observed for the thick Co layers (for nominal thicknesses

above 1.5 nm) and a deviation from this linearity, similar to that of  $M_{\text{eff}}$  (see Fig. 3), is revealed. The trend inversion of  $D_{\text{eff}}$  for thinner Co layers is most probably due to the degradation of the interface quality of the thin ferromagnetic layer. Moreover, this decrease (in absolute value) of  $D_{\text{eff}}$  with decreasing FM effective thickness could be intrinsic since  $D_{\text{eff}}$  should vanish when  $t_{\text{eff}}$  is zero (no magnetic layer). This thickness behavior can be qualitatively reproduced by a toy model as shown in Fig. 5(d). We assume that itinerant electrons in the FM/HM structure behave like free electrons with an effective mass. The dispersion law for electrons in FM is  $\hbar\omega = E_{\text{FM}} + \hbar^2(k_1^2 + k_2^2 + k_3^2)/(2m_{\text{FM}})$ . The dispersion in HM is  $\hbar\omega = E_{\text{HM}} + \hbar^2(k_1^2 + k_2^2 + k_3^2)/(2m_{\text{HM}}) - Jk_2$ . The parameter  $J$  gives an account of SOC, direction 3 is perpendicular to the interface, and direction 1 is parallel to the magnetization direction in FM layer.  $D_{\text{eff}}$  is evaluated as the difference of surface energies for spin parallel to direction 1 in HM or random spin direction in HM. On the other hand, according to first principles calculations, iDMI penetrates into the FM layer [40]. Its effective “penetration depth” includes at least three atomic monolayers (MLs) which means that the contributions of these three nearest MLs are to be taken into account. When the FM thickness drops below the threshold level of three MLs, the contributions of the adjacent second and third atomic layers will gradually disappear from the total iDMI thus weakening the iDMI. It is worth mentioning that the characteristic decrease of the iDMI constant in ultrathin FM films can be regarded as a direct experimental confirmation of the existence of the finite effective iDMI penetration depth. Moreover, its form provides useful information concerning the distribution of the iDMI strength in the vicinity of the FM/HM interface.

The linear fit of the experimental data in Fig. 5(c) allows determining the surface iDMI constant ( $D_s$ ), estimated to be  $(-1.25 \pm 0.05) \times 10^{-7}$  erg/cm. This iDMI surface constant, being slightly higher (in absolute value) than the previously reported value for Pt/Co/Cu ( $-1.05 \times 10^{-7}$  erg/cm) [24] is also lower than the value obtained by Kim *et al.* [41] ( $-1.4 \times 10^{-7}$  erg/cm) for Pt/Co/AlO<sub>x</sub>. This suggests that TaO<sub>x</sub> most probably contributes weakly into the total iDMI in this system. This was confirmed by iDMI measurements on Ta/CoFeB/TaO<sub>x</sub>, where weak  $\Delta F$ , within the BLS limit (below  $\pm 0.1$  GHz), were measured even for maximal  $k_{\text{SW}}$  values and very thin CoFeB films. The obtained values are  $D_{\text{eff}} = -0.015$  erg/cm<sup>2</sup> and  $0.1$  erg/cm<sup>2</sup> for 1.5- and 1.2-nm-thick CoFeB, respectively. This iDMI sign change is not clear but it has been confirmed by probing the dynamics of skyrmionic bubbles, i.e., velocity and direction of motion under the influence of an injected DC current (not shown here), where skyrmionic bubbles are found to move in opposite directions for such CoFeB thicknesses.

## B. Effect of the TaO<sub>x</sub> and spacer thicknesses

In the above investigation, the iDMI in the studied systems may result from both bottom and top interfaces with the ferromagnetic layer, which makes hard the separation of contributions of each interface. Moreover, due to the high iDMI contribution of the Pt/FM interface and owing to the weak total iDMI for Ta/CoFeB/TaO<sub>x</sub>, identifying the role

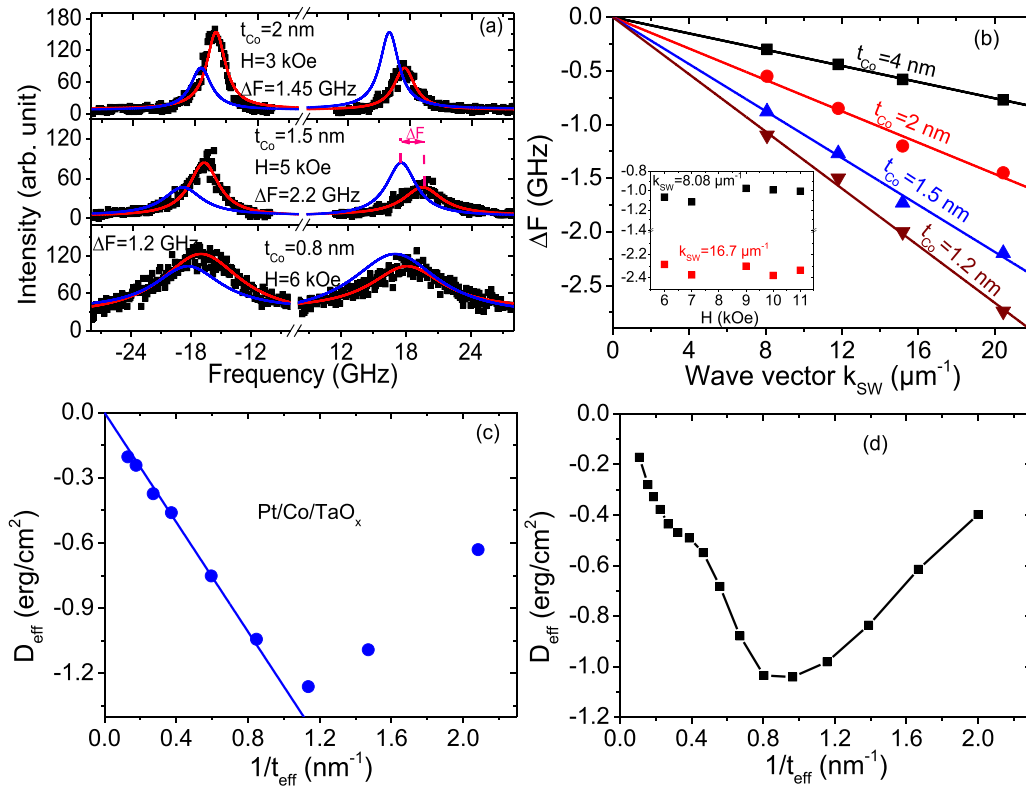


FIG. 5. (a) BLS spectra of Pt/Co/TaO<sub>x</sub> with various Co thicknesses measured at different in-plane positive applied magnetic field values and at a characteristic SW vector  $k_{\text{SW}} = 20.45 \mu\text{m}^{-1}$ . Symbols refer to experimental data, and solid red lines are the Lorentzian fits. Fits corresponding to negative applied magnetic fields are presented in blue lines for clarity and direct comparison of the Stokes and anti-Stokes frequencies. (b) Wave vector ( $k_{\text{SW}}$ ) dependence of the experimental frequency difference  $\Delta F$  of Pt/Co( $t_{\text{Co}}$ )/TaO<sub>x</sub> stacks. Symbols are experimental data and solid lines refer to fit using Eq. (5). The inset shows the experimental frequency difference  $\Delta F$  of Pt/Co(1.2 nm)/TaO<sub>x</sub> stacks as function of the applied magnetic field for given spin wave vector  $k_{\text{SW}}$ . (c) Experimental and (d) simulation of the thickness dependence of the effective iDMI constants of Pt/Co( $t_{\text{Co}}$ )/TaO<sub>x</sub> system. Solid line in (c) refers to the linear fit.

of the FM/TaO<sub>x</sub> interface in iDMI is not clear. Therefore, a powerful method to experimentally elucidate the contribution of the FM/TaO<sub>x</sub> interface to the total iDMI is to vary the thickness and the oxidation state of the TaO<sub>x</sub> and keep the FM layer thickness constant. We should mention that TaO<sub>x</sub> is obtained by *in situ* natural oxidation (see Sec. II) of a given Ta thickness. Therefore, for thinner Ta, the oxygen penetrates the underlying magnetic layer where it diffuses inside it through the grain boundaries, leading to overoxidation. In contrast, optimally oxidized and underoxidized states are obtained by increasing Ta thickness, and thus reducing oxidation at the FM/TaO<sub>x</sub> interface. Figure 6 shows the TaO<sub>x</sub> thickness dependence of  $M_{\text{eff}}$  and  $D_{\text{eff}}$  for Pt/Co(1.2 nm)/TaO<sub>x</sub>( $t$ ) and Ta/CoFeB(1.15 nm)/TaO<sub>x</sub>( $t$ ), where significant changes are observed with the varying TaO<sub>x</sub> thickness/oxidation state, which indicates that the TaO<sub>x</sub> thickness and quality is also a key parameter to tune the PMA and iDMI. Indeed, PMA of Co- and CoFeB-based systems behaves differently: for thin TaO<sub>x</sub> (overoxidized), CoFeB-based structures are perpendicularly magnetized and  $M_{\text{eff}}$  decreases (in absolute value) as TaO<sub>x</sub> thickness increases, suggesting a degradation of PMA. This indicates that thin (0.6 nm) TaO<sub>x</sub> is the optimal oxidation state and thicker Ta leads to underoxidized TaO<sub>x</sub>. In contrast, as TaO<sub>x</sub> thickness increases for Pt/Co/TaO<sub>x</sub> systems, PMA is enhanced and samples are more and more spontaneously

perpendicularly magnetized. This could be explained as follows for Pt/Co/TaO<sub>x</sub>: for thin TaO<sub>x</sub> (overoxidation), Co gets oxidized through penetration of oxygen atoms through the grain boundaries decreasing the exchange coupling between the magnetic grains and hence the overall anisotropy. As TaO<sub>x</sub> increases, oxygen penetrates less and less in the volume of

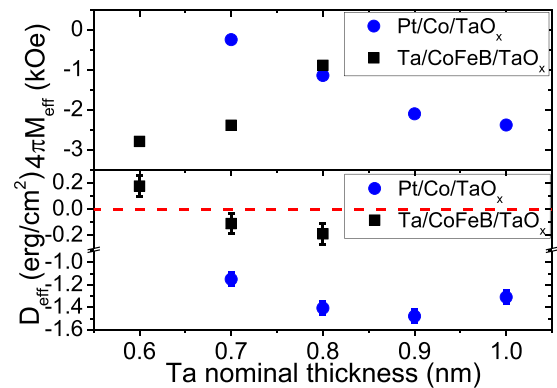


FIG. 6. Variations of the effective magnetization ( $4\pi M_{\text{eff}}$ ) and iDMI constant ( $D_{\text{eff}}$ ) as a function of the Ta nominal thickness and oxidation degree for Pt/Co(1.2 nm)/TaO<sub>x</sub> and Ta/CoFeB(1.15 nm)/TaO<sub>x</sub>.

Co and more and more Co-O bondings are present at the Co/TaO<sub>x</sub> interface, leading to optimal oxidation state and enhancing PMA, as observed by Manchon *et al.* for Pt/Co/AlO<sub>x</sub> [42]. In both cases, the maximum of PMA is observed at the optimum oxidation state, corresponding to an optimum TaO<sub>x</sub> thickness and oxidation level. The different behavior of Ta/CoFeB/TaO<sub>x</sub> is most probably due to the higher magnetic dead layer and the more sensitivity of Fe to the presence of Ta. It seems that the optimal TaO<sub>x</sub> thickness to have PMA is shifted towards lower values, in the case of CoFeB-based systems, due to its high Fe content and the better oxidation of Fe compared to Co. This is consistent with our measurements on double wedge samples (not presented here), where we observe that the optimal oxidation is around 0.6–0.7 nm of Ta for Ta/CoFeB/TaO<sub>x</sub> samples, while it is around 0.9–1 nm for Pt/Co/TaO<sub>x</sub> [28].

Interestingly, in contrast to PMA, the iDMI for both systems shows the same trend. For Ta/CoFeB/TaO<sub>x</sub> and in the thinner Ta region ( $t_{\text{Ta}} = 0.6$  nm), which thus corresponds to the optimally oxidized/overoxidized region, the total  $D_{\text{eff}}$  is positive while it changes its sign and becomes negative for thicker Ta ( $t_{\text{Ta}} \geq 0.7$  nm) in the underoxidized region. As the Ta/CoFeB interface leads to a positive iDMI, we conclude that the overoxidized CoFeB/TaO<sub>x</sub> interface (thin TaO<sub>x</sub>) induces a weak positive or even no iDMI, which becomes negative for a lower oxidation state, i.e., thicker Ta (underoxidized). This behavior is confirmed by the TaO<sub>x</sub> thickness dependence of  $D_{\text{eff}}$  for Pt/Co/TaO<sub>x</sub>, where the total iDMI strength is negative and increases (in absolute value) monotonously as TaO<sub>x</sub> thickness increases, indicating a negative  $D_{\text{eff}}$  of Co/TaO<sub>x</sub> interface for thicker TaO<sub>x</sub> layers. By varying the thickness of the TaO<sub>x</sub> by 0.2 nm (in the range 0.6–0.8 nm for Ta/CoFeB/TaO<sub>x</sub> or in the range 0.7–0.9 nm for Pt/Co/TaO<sub>x</sub>),  $D_{\text{eff}}$  is modulated by 0.35 erg/cm<sup>2</sup>. This behavior proves the contribution of the Co/TaO<sub>x</sub> and CoFeB/TaO<sub>x</sub> interfaces to iDMI mediated by the presence of a Rashba field at the FM/TaO<sub>x</sub> interface [14]. It also offers the possibility to tune the iDMI without changing the FM thickness, which could result in damping increase due to spin pumping. It is difficult to estimate the contribution of the FM/TaO<sub>x</sub> to iDMI, especially from the investigation of the Pt/Co/TaO<sub>x</sub> system due to the large contribution from the Pt/Co bottom interface with relatively spread values in the literature.

For further analysis of the TaO<sub>x</sub> thickness dependence of iDMI induced by the interface with TaO<sub>x</sub>, let us consider the Ta/CoFeB/TaO<sub>x</sub> system, where it is known that the Ta/CoFeB interface leads to a small positive iDMI around 0.03 erg/cm<sup>2</sup> [7,43]. Therefore, we conclude that the optimally oxidized/overoxidized CoFeB/TaO<sub>x</sub> interface (thin TaO<sub>x</sub>) induces a positive iDMI around +0.14 erg/cm<sup>2</sup>. By contrast, the underoxidized interface CoFeB/Ta/TaO<sub>x</sub> leads to a negative iDMI of about −0.2 erg/cm<sup>2</sup>. For the underoxidized interface, we see that the iDMI absolute value is larger when Ta is deposited on top of CoFeB than below. This might be due to the larger intermixed layer due to the stacking order or to the mixed Ta/TaO<sub>x</sub> interface that may be present at this interface. Such change in both sign and magnitude with the increase of TaO<sub>x</sub> thickness has been reported by Arora *et al.* [44] and was attributed to the modification of the degree of

oxygen at the FM interface, thereby affecting the hybridization between 3*d*-2*p* orbitals of FM and oxygen, respectively together with the charge transfer and consequently the iDMI.

A simple physical image of interfacial iDMI remains difficult to define and some fundamental questions, such as those concerning its range and the atomic interface planes involved in this interaction, deserve to be clarified. Moreover, tuning precisely the iDMI constant and PMA is of utmost importance for applications. To address the above-mentioned aspects, Pt (3 nm)/Cu( $t_{\text{Cu}}$ )/Co (1.2 nm)/TaO<sub>x</sub> (0.8 nm)/Al (0.5 nm) with variable  $t_{\text{Cu}}$  in the range 0–2.4 nm were studied. Figure 7(a) shows VSM measurements of the nominal magnetization at saturation, calculated by dividing the magnetic moment to the nominal volume of the Co film (1.2 nm), as a function of  $t_{\text{Cu}}$ . We do not expect a magnetic dead layer at the Cu/Co interface due to the immiscibility of these two materials [45] and thus no intermixing at the Co/Cu interface should be present. Hence, the slow decrease of  $M_s$  with increasing  $t_{\text{Cu}}$  is most probably caused by the decrease of proximity induced magnetization at the Pt/Co interface caused by the inserting Cu. This corresponds to 26% change in film magnetization with respect to that of Cu/Co/TaO<sub>x</sub>.

BLS was used to investigate the variations of  $M_{\text{eff}}$  as a function of the spacer thickness as shown in Fig. 7(b). It reveals that  $M_{\text{eff}}$  increases with increasing  $t_{\text{Cu}}$ , which would suggest a decrease of the perpendicular effective anisotropy field. To further analyze these data, the effective PMA constant ( $K_{\text{eff}} = K_{\perp}$ ) has been calculated, using  $t_{\text{Cu}}$  dependence of  $M_s$ , as presented in Fig. 7(c). Note that for such thin nominal Co layer (1.2 nm) and according to Table I,  $K_v$  is very weak compared to  $K_s/t_{\text{FM}}$  and thus  $K_{\text{eff}}$  mainly reflects the surface anisotropy contribution. As  $t_{\text{Cu}}$  increases, the electron hybridization of Co with Pt at the interface is weaker and weaker and therefore  $K_{\text{eff}}$  decreases. A similar trend was observed for  $D_{\text{eff}}$ , deduced from the spin wave vector dependence of the frequency mismatch, as shown in Fig. 7(d). Here again, as the  $t_{\text{Cu}}$  increases,  $D_{\text{eff}}$  decreases (in absolute value) and then converges towards a nonvanishing positive average value ( $+0.12 \pm 0.05$  erg/cm<sup>2</sup>) corresponding to an iDMI constant of Co(1.2 nm)/TaO<sub>x</sub> (0.8 nm) interface. This value is in good agreement with the obtained value for optimally oxidized CoFeB/TaO<sub>x</sub> (0.6 nm) as shown above.

For a deep analysis of data, we phenomenologically fitted the experimental data of  $K_{\text{eff}}$  and  $D_{\text{eff}}$  in Figs. 7(c) and 7(d) with an exponential decay function ( $A_0 + A_1 e^{-t_{\text{Cu}}/\lambda}$ , where  $A_0$ ,  $A_1$ , and  $\lambda$  are the fit parameters). This allows us to quantitatively compare the characteristic decay thicknesses ( $\lambda$ ) of  $D_{\text{eff}}$  and  $K_{\text{eff}}$ . The obtained values of  $\lambda$  are found to be 0.35 and 0.21 nm for PMA and iDMI constants, respectively. It corresponds roughly to one or two atomic monolayers thickness, thus suggesting that these interface SOC-related quantities are very localized at the first interface atomic monolayers with the heavy metal. We may thus conclude that one atomic Cu layer is sufficient to significantly screen the Pt layer and reduce its contribution to iDMI and PMA. Nevertheless, it is worth mentioning the thinner decay length for iDMI compared to PMA most probably due to the greater restriction of iDMI to the first atoms at interfaces. Furthermore, the obtained values of  $A_1$  from the fit of experimental data in Figs. 7(c) and 7(d) characterize the strength of PMA and iDMI at the Pt/Co

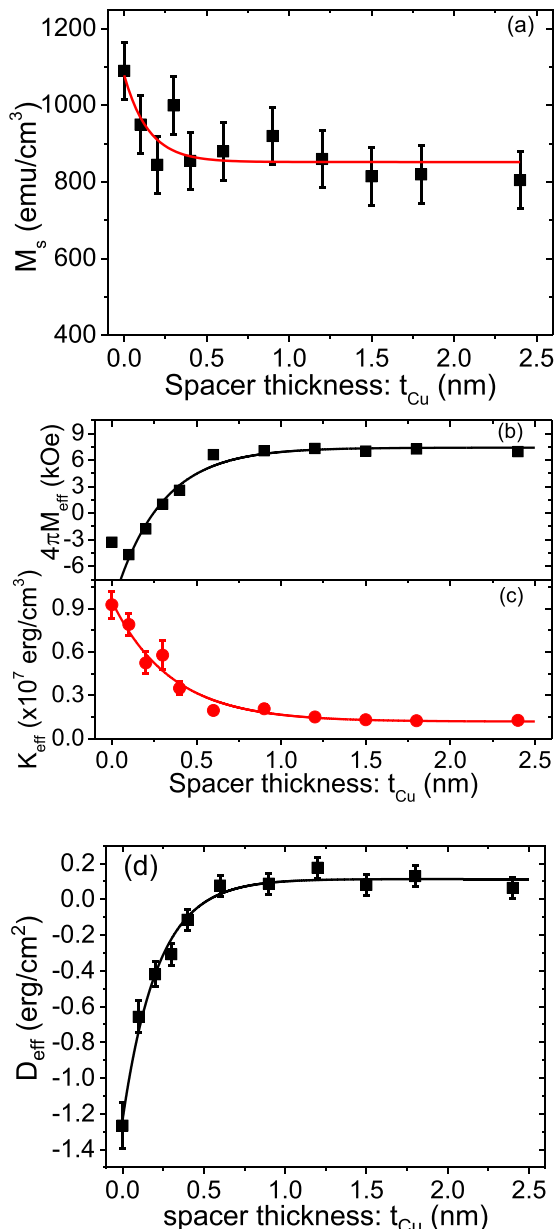


FIG. 7. Variations of (a) the magnetization at saturation ( $M_s$ ), (b) the effective magnetization ( $4\pi M_{\text{eff}}$ ) measured by BLS, (c) the perpendicular effective anisotropy constant ( $K_{\text{eff}}$ ), and (d) the effective iDMI constant ( $D_{\text{eff}}$ ) vs the Cu spacer thickness for Pt/Cu/Co(1.2 nm)/TaO<sub>x</sub> (0.8 nm)/Al. Symbols are experimental data and solid lines refer to fits with exponential decay function ( $A_0 + A_1 e^{-t_{\text{Cu}}/\lambda}$ , where  $A_0$ ,  $A_1$ , and  $\lambda$  are the fit parameters).

(1.2 nm) and can be used to estimate  $K_s$  and  $D_s$  for the Pt/Co interface. Therefore the obtained values, using the nominal thickness of Co (1.2 nm) are found to be  $K_s = 1.1 \text{ erg/cm}^2$  and  $D_s = -1.6 \times 10^{-7} \text{ erg/cm}$ . The comparison with the corresponding values of Pt/Co/TaO<sub>x</sub> summarized in Table I (obtained in Sec. III A) confirms that in such systems both iDMI and PMA are induced by the Pt/Co interface. It is worth mentioning that the fit parameter  $A_0$  characterizes the iDMI and the PMA strength of Cu/Co/TaO<sub>x</sub>, which is found to be significantly lower than those of the Pt/Co interface.

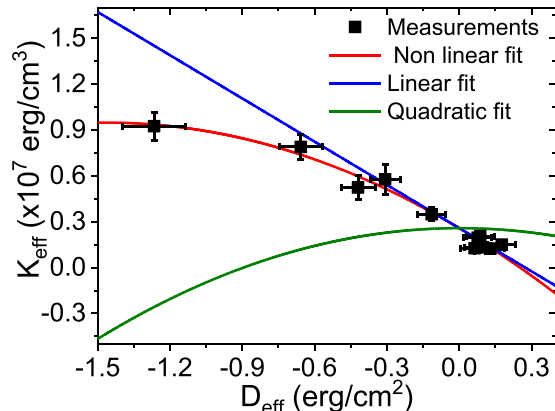


FIG. 8. Variations of the perpendicular effective magnetic anisotropy constant ( $K_{\text{eff}}$ ) as a function of the effective iDMI constant ( $D_{\text{eff}}$ ) for Pt/Cu/Co(1.2 nm)/TaO<sub>x</sub> (0.8 nm)/Al with a variable Cu thickness. Symbols refer to experimental data, the solid blue line is the pure linear fit ( $K_{\text{eff}} = 2.58 \times 10^6 - 9.43 \times 10^6 D_{\text{eff}}$ ), the solid olive line is the pure quadratic fit ( $K_{\text{eff}} = 2.58 \times 10^6 - 3.22 \times 10^6 D_{\text{eff}}^2$ ), and the solid red line is fit with equation:  $K_{\text{eff}} = 2.58 \times 10^6 - 9.43 \times 10^6 D_{\text{eff}} - 3.22 \times 10^6 D_{\text{eff}}^2$ .

We finally investigated the correlation between iDMI and PMA for the Pt/Cu/Co/TaO<sub>x</sub> system by plotting  $K_{\text{eff}}$  as a function of  $D_{\text{eff}}$  as shown in Fig. 8. This latter shows an evident correlation between iDMI and PMA which manifests itself by a nonlinear (mixture between linear and quadratic: second-degree polynomial function) dependence between  $K_{\text{eff}}$  and  $D_{\text{eff}}$ , suggesting their common origin, namely  $3d$ - $5d$  orbital hybridization of Co and Pt. As shown in Fig. 8, taking only a pure linear relation between  $K_{\text{eff}}$  and  $D_{\text{eff}}$ , one obtains the blue curve, which fits nicely the experimental data in the  $D_{\text{eff}}$  range of  $-0.4 \leq D_{\text{eff}} \leq 0.2 \text{ erg/cm}^2$  ( $0.3 \text{ nm} \leq t_{\text{Cu}} \leq 2.4 \text{ nm}$ ), where the SOC is weak. The data in the range  $-1.26 \text{ erg/cm}^2 \leq D_{\text{eff}} < -0.4 \text{ erg/cm}^2$ , corresponding to a thinner spacers ( $t_{\text{Cu}} = 0$ – $0.2 \text{ nm}$ ), are not matching the linear fits and cannot be outlier. The iDMI constant in this range is high due to the fact that the contribution of Pt is not completely screened by the spacer (Cu). Moreover, further measurements in this region are not possible since the spacer thickness cannot be changed with a step below 0.1 nm. This again proves that iDMI is very sensitive to the first atomic monolayers at the interfaces. It is thus clear that the linear dependence alone is not sufficient to describe the correlation within the whole range of  $D_{\text{eff}}$ . In particular, for higher  $D_{\text{eff}}$  absolute values (i.e., for  $0 \leq t_{\text{Cu}} \leq 0.3 \text{ nm}$ : higher SOC), a nonlinear (quadratic) dependence should be added to the linear function to account for the fit of the full variation of  $K_{\text{eff}}$  versus  $D_{\text{eff}}$ . Therefore the experimental data have been fitted by considering a second-degree polynomial function (straight red color line in Fig. 8). We should mention that a quadratic dependence is theoretically predicted from perturbation theories for PMA [46] and iDMI [47], since iDMI energy results from the first order of the SOC, while the interface PMA comes from its second order. However, a linear correlation between  $K_s$  and  $D_{\text{eff}}$  has been reported experimental in Pt/Co/AlO<sub>x</sub> system from the study of the dependence of the two quantities on the Pt thickness [48]. This linear behavior was attributed to the narrow variation range of

PMA and/or iDMI in which the correlation is investigated, as we observed for  $0.3 \text{ nm} \leq t_{\text{Cu}} \leq 2.4 \text{ nm}$ . Therefore, the mixture between the pure linear and quadratic dependencies is in good agreement with these trends and proves the correlation between PMA and iDMI. It is worth mentioning that in Pt/Cu/Co/TaO<sub>x</sub> systems with variable Cu thickness, the contribution of the top interface (Co/TaO<sub>x</sub>) to both iDMI and interface anisotropy is fixed and any change in effective iDMI and anisotropy results most probably from the contribution of the bottom interface with Co (Pt/Cu/Co). Therefore, origins of these two quantities are more correlated. We thus conclude that the modulation of iDMI and PMA by insertion of spacer layer between the HM and FM layers remains a powerful method to investigate their correlation since it clarifies their origin, especially for the interface PMA, where both interfaces could contribute and could change when varying FM thickness. Moreover, this nonlinear dependence of  $K_{\text{eff}}$  as a function of  $D_{\text{eff}}$  could result from the different characteristic decay thicknesses between iDMI and PMA: iDMI is more localized at the first interface as revealed above.

#### IV. CONCLUSION

Perpendicular magnetic anisotropy, iDMI, and Gilbert damping of Pt/Co/TaO<sub>x</sub> and Ta/CoFeB/TaO<sub>x</sub> have been

investigated versus Co, CoFeB, and TaO<sub>x</sub> thicknesses and oxidation level. When varying the Co and CoFeB thicknesses for each system BLS and MS-FMR were used to evidence a strong iDMI, PMA, and spin mixing conductance for Pt/Co/TaO<sub>x</sub> and a weak iDMI, a slightly lower PMA, and a smaller damping for Ta/CoFeB/TaO<sub>x</sub>. Moreover, Co/TaO<sub>x</sub> and CoFeB/TaO<sub>x</sub> are found to induce iDMI, mediated by the presence of a Rashba field at the interface with TaO<sub>x</sub>, which can be modulated in sign and in strength by varying the TaO<sub>x</sub> thickness and oxidation level. By inserting a Cu layer between Pt and Co layers, we demonstrate that PMA and iDMI can be significantly modulated and we evidenced a nonlinear correlation between  $D_{\text{eff}}$  and  $K_{\perp}$ . This nonlinear dependence could be attributed to the similar interface orbital hybridizations involved in PMA and iDMI. Furthermore, we prove that iDMI and interface PMA are induced by the first interface monolayers of Pt.

#### ACKNOWLEDGMENTS

This work has been supported by the Conseil regional d'Île-de-France (convention 1763) through the DIM NanoK (BIDUL project) and by the French ANR (Contract ELEC-SPIN No. ANR-16-CE24-0018 and Contract ADMIS No. ANR-19-CE24-0019).

- 
- [1] A. Hoffmann and S. D. Bader, *Phys. Rev. Appl.* **4**, 047001 (2015).
- [2] J. Sinova, S. O. Valenzuela, J. Wunderlich, C. H. Back, and T. Jungwirth, *Rev. Mod. Phys.* **87**, 1213 (2015).
- [3] A. Fert, N. Reyren, and V. Cros, *Nat. Rev. Mater.* **2**, 17031 (2017).
- [4] F. Hellman, A. Hoffmann, Y. Tserkovnyak, G. S. D. Beach, E. E. Fullerton, C. Leighton, A. H. MacDonald, D. C. Ralph, D. A. Arena, H. A. Dürr, P. Fischer, J. Grollier, J. P. Heremans, T. Jungwirth, A. V. Kimel, B. Koopmans, I. N. Krivorotov, S. J. May, A. K. Petford-Long, J. M. Rondinelli *et al.*, *Rev. Mod. Phys.* **89**, 025006 (2017).
- [5] J. Zang, V. Cros, and A. Hoffmann, in *Solid State Sciences* (Springer, New York, 2018), pp. 1–176.
- [6] A. Belabbes, G. Bihlmayer, F. Bechstedt, S. Blügel, and A. Manchon, *Phys. Rev. Lett.* **117**, 247202 (2016).
- [7] X. Ma, G. Yu, C. Tang, X. Li, C. He, J. Shi, K. L. Wang, and X. Li, *Phys. Rev. Lett.* **120**, 157204 (2018).
- [8] I. Dzyaloshinsky, *J. Phys. Chem. Solids* **4**, 241 (1958).
- [9] T. Moriya, *Phys. Rev. Lett.* **4**, 228 (1960).
- [10] A. Fert and P. M. Levy, *Phys. Rev. Lett.* **44**, 1538 (1980).
- [11] A. Fert, V. Cros, and J. Sampaio, *Nat. Nanotechnol.* **8**, 152 (2013).
- [12] A. R. Fert, *Mater. Sci. Forum* **59-60**, 439 (1991).
- [13] Y. A. Bychkov and E. I. Rashba, *JETP Lett.* **39**, 78 (1984).
- [14] K. W. Kim, H. W. Lee, K. J. Lee, and M. D. Stiles, *Phys. Rev. Lett.* **111**, 216601 (2013).
- [15] T. Srivastava, M. Schott, R. Juge, V. Krizakova, M. Belmeguenai, Y. Roussigne, A. Bernard-Mantel, L. Ranno, S. Pizzini, S-M. Chérif, A. Stashkevich, S. Auffret, O. Boulle, G. Gaudin, M. Chshiev, C. Baraduc, and H. Béa, *Nano Lett.* **18**, 4871 (2018).
- [16] C. Kim, D. Kim, B. S. Chun, K-W. Moon, and C. Hwang, *Phys. Rev. Appl.* **9**, 054035 (2018).
- [17] S. Tacchi, R. E. Troncoso, M. Ahlberg, G. Gubbiotti, M. Madami, J. Åkerman, and P. Landeros, *Phys. Rev. Lett.* **118**, 147201 (2017).
- [18] R. M. Rowan-Robinson, A. A. Stashkevich, Y. Roussigne, M. Belmeguenai, S-M. Chérif, A. Thiaville, T. P. A. Hase, A. T. Hindmarch, and D. Atkinson, *Sci. Rep.* **7**, 16835 (2017).
- [19] N-H. Kim, J. Cho, J. Jung, D-S. Han, Y. Yin, J-S. Kim, H. J. M. Swagten, K. Lee, M-H. Jung, and C-Y. You, *AIP Adv.* **7**, 035213 (2017).
- [20] W. Jiang, P. Upadhyaya, W. Zhang, G. Yu, M. B. Jungfleisch, F. Y. Fradin, J. E. Pearson, Y. Tserkovnyak, K. L. Wang, O. Heinonen, S. G. E. te Velthuis, and A. Hoffmann, *Science* **349**, 283 (2015).
- [21] M. Belmeguenai, H. Tuzcuoglu, M. S. Gabor, T. Petrisor, Jr., C. Tiusan, D. Berling, F. Zighem, T. Chauveau, S. M. Chérif, and P. Moch, *Phys. Rev. B* **87**, 184431 (2013).
- [22] M. Belmeguenai, M. S. Gabor, Y. Roussigné, A. Stashkevich, S. M. Chérif, F. Zighem, and C. Tiusan, *Phys. Rev. B* **93**, 174407 (2016).
- [23] H. K. Gweon, S. J. Yun, and S. H. Lim, *Sci. Rep.* **8**, 1266 (2018).
- [24] M. Belmeguenai, Y. Roussigné, S-M. Chérif, A. Stashkevich, T. Petrisor, Jr., M. Nasui, and M. S. Gabor, *J. Phys. D: Appl. Phys.* **52**, 125002 (2019).
- [25] N. Vernier, J-P Adam, S. Eimer, G. Agnus, T. Devolder, Thomas Hauet, B. Ocker, F. Garcia, and D. Ravelosona, *Appl. Phys. Lett.* **104**, 122404 (2014).
- [26] X. Liu, W. Zhang, M. J. Carter, and G. Xiao, *J. Appl. Phys.* **110**, 033910 (2011).
- [27] T. Ogasawara, M. Oogane, M. Al-Mahdawi, M. Tsunoda, and Y. Ando, *AIP Adv.* **9**, 125053 (2019).

- [28] T. Srivastava, W. Lim, I. Joumard, S. Auffret, C. Baraduc, and H. Béa, *Phys. Rev. B* **100**, 220401(R) (2019).
- [29] M. Belmeguenai, K. Aitoukaci, F. Zighem, M. S. Gabor, T. Petrisor, R. B. Mos, and C. Tiusan, *J. Appl. Phys.* **123**, 113905 (2018).
- [30] M. Belmeguenai, Y. Roussigné, H. Bouloussa, S. M. Chérif, A. Stashkevich, M. Nasui, M. S. Gabor, A. Mora-Hernández, B. Nicholson, O.-O. Inyang, A. T. Hindmarch, and L. Bouchenoire, *Phys. Rev. Appl.* **9**, 044044 (2018).
- [31] P. J. Chen, Y. L. Iunin, S. F. Cheng, and R. D. Shull, *IEEE Trans. Magn.* **52**, 4400504 (2016).
- [32] J. Camarero, J. J. de Miguel, R. Miranda, V. Raposo, and A. Hernando, *Phys. Rev. B* **64**, 125406 (2001).
- [33] J. Ye, W. He, Q. Wu, H.-L. Liu, X.-Q. Zhang, Z.-Y. Chen, and Z.-H. Cheng, *Sci. Rep.* **3**, 2148 (2013).
- [34] H. Nakayama, K. Ando, K. Harii, T. Yoshino, R. Takahashi, Y. Kajiwara, K. Uchida, Y. Fujikawa, and E. Saitoh, *Phys. Rev. B* **85**, 144408 (2012).
- [35] T. Devolder, T. Tahmasebi, S. Eimer, T. Hauet, and S. Andrieu, *Appl. Phys. Lett.* **103**, 242410 (2013).
- [36] T. Devolder, P.-H. Ducrot, J.-P. Adam, I. Barisic, N. Vernier, J.-V. Kim, B. Ockert, and D. Ravelosona, *Appl. Phys. Lett.* **102**, 022407 (2013).
- [37] W. Zhang, W. Han, X. Jiang, S.-H. Yang, and S. S. P. Parkin, *Nat. Phys.* **11**, 496 (2015).
- [38] C.-F. Pai, Y. Ou, L. H. Vilela-Leão, D. C. Ralph, and R. A. Buhrman, *Phys. Rev. B* **92**, 064426 (2015).
- [39] X. Tao, Q. Liu, B. Miao, R. Yu, Z. Feng, L. Sun, B. You, J. Du, K. Chen, S. Zhang, L. Zhang, Z. Yuan, D. Wu, and H. Ding, *Sci. Adv.* **4**, eaat1670 (2018).
- [40] H. Yang, A. Thiaville, S. Rohart, A. Fert, and M. Chshiev, *Phys. Rev. Lett.* **115**, 267210 (2015).
- [41] N.-H. Kim, J. Jung, J. Cho, D.-S. Han, Y. Yin, J.-S. Kim, H. J. M. Swagten, and C.-Y. You, *Appl. Phys. Lett.* **108**, 142406 (2016).
- [42] A. Manchon, C. Ducruet, L. Lombard, S. Auffret, B. Rodmacq, B. Dieny, S. Pizzini, J. Vogel, V. Uhlř, M. Hochstrasser, and G. Panaccione, *J. Appl. Phys.* **104**, 043914 (2008).
- [43] L. Herrera Diez, M. Voto, A. Casiraghi, M. Belmeguenai, Y. Roussigné, G. Durin, A. Lamperti, R. Mantovan, V. Sluka, V. Jeudy, Y. T. Liu, A. Stashkevich, S. M. Chérif, J. Langer, B. Ocker, L. Lopez-Diaz, and D. Ravelosona, *Phys. Rev. B* **99**, 054431 (2019).
- [44] S. Bandiera, R. C. Sousa, B. Rodmacq, and B. Dieny, *IEEE Magn. Lett.* **2**, 3000504 (2011).
- [45] M. Arora, J. M. Shaw, and H. T. Nembach, *Phys. Rev. B* **101**, 054421 (2020).
- [46] P. Bruno, *Phys. Rev. B* **39**, 865 (1989).
- [47] M. Heide, G. Bihlmayer, and S. Blügel, *Physica B (Amsterdam, Neth.)* **404**, 2678 (2009).
- [48] N.-H. Kim, D.-S. Han, J. Jung, K. Park, H. J. M. Swagten, J.-S. Kim, and C.-Y. You, *Appl. Phys. Express* **10**, 103003 (2017).